

Strong variability of the coronal line region in NGC 5548

Hermine Landt^{1*}†, Martin J. Ward^{1†}, Katrien C. Steenbrugge² and Gary J. Ferland^{3,4}

¹*Department of Physics, Durham University, South Road, Durham DH1 3LE, UK*

²*Instituto de Astronomía, Universidad Católica del Norte, Avenida Angamos 0610, 1270709 Antofagasta, Chile*

³*School of Mathematics and Physics, Queen's University of Belfast, Belfast BT7 1NN, Northern Ireland, UK*

⁴*Department of Physics and Astronomy, University of Kentucky, Lexington, KY 40506, USA*

Accepted . Received ; in original form

ABSTRACT

We present the second extensive study of the coronal line variability in an active galaxy. Our data set for the well-studied Seyfert galaxy NGC 5548 consists of five epochs of quasi-simultaneous optical and near-infrared spectroscopy spanning a period of about five years and three epochs of X-ray spectroscopy overlapping in time with it. Whereas the broad emission lines and hot dust emission varied only moderately, the coronal lines varied strongly. However, the observed high variability is mainly due to a flux decrease. Using the optical [Fe VII] and X-ray O VII emission lines we estimate that the coronal line gas has a relatively low density of $n_e \sim 10^3 \text{ cm}^{-3}$ and a relatively high ionisation parameter of $\log U \sim 1$. The resultant distance of the coronal line gas from the ionising source of about eight light years places this region well beyond the hot inner face of the dusty torus. These results imply that the coronal line region is an independent entity. We find again support for the X-ray heated wind scenario of Pier & Voit; the increased ionising radiation that heats the dusty torus also increases the cooling efficiency of the coronal line gas, most likely due to a stronger adiabatic expansion. The much stronger coronal line variability of NGC 5548 relative to that of NGC 4151 can also be explained within this picture. NGC 5548 has much stronger coronal lines relative to the low ionisation lines than NGC 4151 indicating a stronger wind, in which case a stronger adiabatic expansion of the gas and so fading of the line emission is expected.

Key words: galaxies: Seyfert – infrared: galaxies – X-rays: galaxies – quasars: emission lines – quasars: individual: NGC 5548

1 INTRODUCTION

In addition to the broad and narrow emission lines, the spectra of active galactic nuclei (AGN) display high-ionisation emission lines, the so-called coronal lines, which require energies $\gtrsim 100 \text{ eV}$ to be excited. The coronal line region is believed to lie at distances from the central ionising source intermediate between those of the broad (BELR) and narrow emission line region (NELR) and to possibly coincide with the hot inner face of the circumnuclear, obscuring dusty torus (as first suggested by Pier & Voit 1995). This assumption is based mainly on the following: (i) the coro-

nal lines have 3 – 4 orders of magnitude higher critical densities for collisional deexcitation than the low-ionisation narrow emission lines and are believed to be emitted at these densities; (ii) the coronal line profiles often but not always have full widths at half maxima (FWHM) intermediate between those of the broad and narrow emission lines ($\text{FWHM} \sim 500 - 1500 \text{ km s}^{-1}$; e.g., Penston et al. 1984; Appenzeller & Oestreicher 1988; Erkens et al. 1997; Rodríguez-Ardila et al. 2002, 2011); and (iii) the emission from this region is often extended but much less so than that from the low-ionisation NELR (on scales of $\sim 80 - 150 \text{ pc}$; e.g., Prieto et al. 2005; Müller Sánchez et al. 2006; Müller-Sánchez et al. 2011; Mazzalay et al. 2013). Recently, Rose et al. (2015) found evidence in their study of seven AGN with strong coronal lines selected from the Sloan Digital Sky Survey (SDSS) that the coronal line region has higher densities than the low-ionisation NELR and lies at distances from the ionising source similar to those estimated for the hot dust sublimation radius.

* E-mail: hermine.landt@durham.ac.uk

† Visiting Astronomer at the Infrared Telescope Facility, which is operated by the University of Hawaii under Cooperative Agreement no. NNX-08AE38A with the National Aeronautics and Space Administration, Science Mission Directorate, Planetary Astronomy Program.

In Landt et al. (2015), we have presented the first extensive study of the coronal line variability in an AGN and have started to question this picture. Our data set for the nearby, well-known source NGC 4151 included six epochs of quasi-simultaneous optical and near-IR spectroscopy spanning a period of ~ 8 years and five epochs of X-ray spectroscopy overlapping in time with it, with the observations in each wavelength performed with the same telescope and set-up. For this source we found that the coronal lines varied only weakly, if at all, and estimated a relatively low density ($n_e \sim 10^3 \text{ cm}^{-3}$) and high ionisation parameter ($\log U \sim 1$) for the coronal line gas. The resultant distance of the coronal line region from the ionising continuum was ~ 2 light years, which is well beyond the hot inner face of the obscuring torus of (~ 2 light months; Koshida et al. 2014). Based on the high ionisation parameter, we proposed that the coronal line region is an independent entity rather than part of a continuous gas distribution connecting the BELR and low-ionisation NELR, possibly an X-ray heated wind as suggested by Pier & Voit (1995).

The most stringent constraints on the properties of the coronal line emitting region could come from variability studies, in particular if the variability of several coronal lines can be compared with each other and with that of other AGN components such as the BELR, hot dust emission and X-ray luminosity, as we have done in Landt et al. (2015). However, mainly due to the weakness of these emission lines and also lack of data, very few studies of this kind have been attempted so far. Veilleux (1988) made the only systematic study of the coronal line variability. In his sample of ~ 20 AGN he found firm evidence that both the [Fe VII] $\lambda 6087$ and [Fe X] $\lambda 6375$ emission lines varied (during a period of a few years) for only one source, namely, NGC 5548, which is the subject of this paper, and tentative evidence for another seven sources (including NGC 4151). Then, within a general optical variability campaign on the source Mrk 110 lasting for half a year, Kollatschny et al. (2001) reported strong [Fe X] variations. More recently, follow-up optical spectroscopy of a handful of objects with unusually prominent coronal lines selected from the SDSS showed that in half of them the coronal lines strongly faded (by factors of $\sim 2 - 10$), making these sources candidates for stellar tidal disruption events (Komossa et al. 2009; Yang et al. 2013).

Here we present the second extensive study of the coronal line variability in an AGN. Our data set for the well-studied source NGC 5548 ($z = 0.017$) consists of five epochs of quasi-simultaneous optical and near-infrared spectroscopy spanning a period of ~ 5 years and three epochs of X-ray spectroscopy overlapping in time with it. The paper is organised as follows. In Section 2, we present the data and measurements. In Section 3, we discuss the observed variability behaviour of the near-IR, optical and X-ray coronal lines, for which we seek an interpretation in the context of the location of and excitation mechanism for the coronal line emission region in Section 4. Finally, in Section 5, we summarise our main results and present our conclusions. Throughout this paper we have assumed cosmological parameters $H_0 = 70 \text{ km s}^{-1} \text{ Mpc}^{-1}$, $\Omega_M = 0.3$, and $\Omega_\Lambda = 0.7$.

2 THE DATA AND MEASUREMENTS

2.1 Near-IR and optical spectroscopy

We have five epochs of quasi-simultaneous (within less than two months) near-IR and optical spectroscopy for NGC 5548 (see Tables 1 and 2). All data are of relatively high signal-to-noise ratio (continuum $S/N \gtrsim 50 - 100$). The near-IR spectroscopy was obtained with the SpeX spectrograph (Rayner et al. 2003) at the NASA Infrared Telescope Facility (IRTF), a 3 m telescope on Mauna Kea, Hawai'i, in the short cross-dispersed mode (SXD, $0.8 - 2.4 \mu\text{m}$). All data were obtained through a slit of $0.8 \times 15''$ giving an average spectral resolution of full width at half maximum (FWHM) $\sim 400 \text{ km s}^{-1}$. The four epochs spanning the years 2004 – 2007 are our own data and were discussed and presented in Landt et al. (2008) and Landt et al. (2011). The near-IR spectrum from 2002 was discussed by Riffel et al. (2006). The optical spectra were obtained with the FAST spectrograph (Fabricant et al. 1998) at the Tillinghast 1.5 m telescope on Mt. Hopkins, Arizona, using the 300 l/mm grating and a $3''$ long-slit. This set-up resulted in a wavelength coverage of $\sim 3720 - 7515 \text{ \AA}$ and an average spectral resolution of FWHM $\sim 330 \text{ km s}^{-1}$. The slit was rotated to the parallactic angle for all observations but the May 2004 epoch. However, the latter spectrum was observed at a very low air mass ($\sec z \sim 1.01$). The optical data were discussed and presented in Landt et al. (2008) and Landt et al. (2011), with the exception of the May 2004 spectrum, which was retrieved from the FAST archive.

We have measured the fluxes of the strongest near-IR and optical coronal lines and estimated their 1σ uncertainties as detailed in Landt et al. (2015). In the near-IR, we have measured two sulfur lines and two silicon lines, namely, [S VIII] $\lambda 9911$, [S IX] $1.252 \mu\text{m}$, [Si VI] $1.965 \mu\text{m}$ and [Si X] $1.430 \mu\text{m}$ (see Table 1). In the optical, we have measured four iron emission lines, namely, [Fe VII] $\lambda 3759$, [Fe VII] $\lambda 5159$, [Fe VII] $\lambda 5721$ and [Fe VII] $\lambda 6087$ (see Table 2). The 1σ uncertainties are $\sim 1 - 5\%$ for the strongest lines and $\sim 2 - 20\%$ for the weakest ones. Since the spectra were obtained in non-photometric sky conditions, we study in the following the temporal changes of the coronal lines in relative rather than absolute flux. In particular, we scale the coronal line emission to that of a strong, forbidden *low-ionisation* emission line that is unblended and observed in the same spectrum. The emission region that produces the low-ionisation narrow lines is believed to be located at large enough distances from the central ionising source (e.g. Pogge 1988; Tadhunter & Tsvetanov 1989) and to have a relatively low density for its flux to remain constant on timescales of decades. We have scaled the near-IR and optical coronal lines to the [S III] $\lambda 9531$ and [O III] $\lambda 5007$ emission lines, respectively.

In order to further constrain the significance of the observed coronal line variability, we have considered the two extreme cases of where no variability and the highest variability are expected. For both scaling lines we observe also the other emission line that is emitted from the same upper level, namely, [S III] $\lambda 9069$ and [O III] $\lambda 4959$. Their observed ratios, which should be close to the theoretical values of [S III] $\lambda 9531/\lambda 9069 = 2.58$ and [O III] $\lambda 5007/\lambda 4959 = 2.92$ (Kramida et al. 2013), are not expected to vary and so their observed variability sets a lower threshold for the signifi-

Table 1. Near-IR emission line fluxes and ratios

Observation Date	[S III] $\lambda 9531$ (erg/s/cm ²)	[S III] $\lambda 9069$ (erg/s/cm ²)	[S III]/ [S III]	[S VIII] $\lambda 9911$ (erg/s/cm ²)	[S III]/ [S VIII]	[S IX] $1.252\mu\text{m}$ (erg/s/cm ²)	[S III]/ [S IX]
2002 Apr 23	(2.79 \pm 0.06)e-14	(1.24 \pm 0.04)e-14	2.25 \pm 0.09	(4.45 \pm 0.17)e-15	6.3 \pm 0.3	(2.88 \pm 0.17)e-15	9.7 \pm 0.6
2004 May 23	(4.50 \pm 0.11)e-14	(1.76 \pm 0.11)e-14	2.56 \pm 0.17	(4.02 \pm 0.76)e-15	11.2 \pm 2.1	(2.60 \pm 0.99)e-15	17.3 \pm 6.6
2006 Jan 9	(3.86 \pm 0.22)e-14	(1.79 \pm 0.11)e-14	2.16 \pm 0.18	(5.22 \pm 0.73)e-15	7.4 \pm 1.1	(4.44 \pm 0.93)e-15	8.7 \pm 1.9
2006 Jun 12	(6.49 \pm 0.15)e-14	(2.65 \pm 0.19)e-14	2.45 \pm 0.19	(4.89 \pm 0.55)e-15	13.3 \pm 1.5	(3.79 \pm 0.55)e-15	17.1 \pm 2.5
2007 Jan 24	(5.36 \pm 0.10)e-14	(1.96 \pm 0.07)e-14	2.74 \pm 0.11	(4.23 \pm 0.53)e-15	12.7 \pm 1.6	(2.73 \pm 0.29)e-15	19.6 \pm 2.1
Observation Date	[S III] $\lambda 9531$ (erg/s/cm ²)	[Si VI] $1.965\mu\text{m}$ (erg/s/cm ²)	[S III]/ [Si VI]	[Si X] $1.430\mu\text{m}$ (erg/s/cm ²)	[S III]/ [Si X]	Pa β (erg/s/cm ²)	[S III]/ Pa β
2002 Apr 23	(2.79 \pm 0.06)e-14	(1.42 \pm 0.02)e-14	2.0 \pm 0.1	(6.57 \pm 0.21)e-15	4.3 \pm 0.2	(6.90 \pm 0.10)e-14	0.404 \pm 0.011
2004 May 23	(4.50 \pm 0.11)e-14	(1.30 \pm 0.18)e-14	3.5 \pm 0.5	(1.19 \pm 0.12)e-14	3.8 \pm 0.4	(1.11 \pm 0.04)e-13	0.405 \pm 0.017
2006 Jan 9	(3.86 \pm 0.22)e-14	(1.32 \pm 0.05)e-14	2.9 \pm 0.2	(3.38 \pm 0.55)e-15	11.4 \pm 2.0	(1.26 \pm 0.03)e-13	0.306 \pm 0.020
2006 Jun 12	(6.49 \pm 0.15)e-14	(2.27 \pm 0.07)e-14	2.9 \pm 0.1	(5.86 \pm 0.45)e-15	11.1 \pm 0.9	(1.68 \pm 0.05)e-13	0.386 \pm 0.015
2007 Jan 24	(5.36 \pm 0.10)e-14	(1.01 \pm 0.04)e-14	5.3 \pm 0.2	(3.61 \pm 0.23)e-15	14.9 \pm 1.0	(1.37 \pm 0.02)e-13	0.391 \pm 0.010

Table 2. Optical emission line fluxes and ratios

Observation Date	[O III] $\lambda 5007$ (erg/s/cm ²)	[O III] $\lambda 4959$ (erg/s/cm ²)	[O III]/ [O III]	[Fe VII] $\lambda 3759$ (erg/s/cm ²)	[O III]/ [Fe VII]	[Fe VII] $\lambda 5159$ (erg/s/cm ²)	[O III]/ [Fe VII]
2002 Mar 6	(4.72 \pm 0.06)e-13	(1.51 \pm 0.06)e-13	3.13 \pm 0.13	(1.94 \pm 0.24)e-14	24.3 \pm 3.1	(1.11 \pm 0.20)e-14	42.5 \pm 7.5
2004 May 24	(5.21 \pm 0.05)e-13	(1.90 \pm 0.07)e-13	2.74 \pm 0.10	(1.94 \pm 0.20)e-14	26.9 \pm 2.8	(1.29 \pm 0.14)e-14	40.4 \pm 4.4
2006 Jan 9	(5.89 \pm 0.02)e-13	(2.01 \pm 0.03)e-13	2.93 \pm 0.05	(1.37 \pm 0.13)e-14	43.0 \pm 4.1	(8.31 \pm 1.01)e-15	70.9 \pm 8.6
2006 Jun 20	(4.19 \pm 0.04)e-13	(1.40 \pm 0.02)e-13	2.99 \pm 0.06	(1.85 \pm 0.19)e-14	22.7 \pm 2.3	(9.03 \pm 1.00)e-15	46.4 \pm 5.2
2007 Feb 17	(2.97 \pm 0.03)e-13	(9.71 \pm 0.24)e-14	3.06 \pm 0.08	(8.76 \pm 1.24)e-15	33.9 \pm 4.8	(5.04 \pm 0.71)e-15	58.9 \pm 8.3
Observation Date	[O III] $\lambda 5007$ (erg/s/cm ²)	[Fe VII] $\lambda 5721$ (erg/s/cm ²)	[O III]/ [Fe VII]	[Fe VII] $\lambda 6087$ (erg/s/cm ²)	[O III]/ [Fe VII]	H α (erg/s/cm ²)	[O III]/ H α
2002 Mar 6	(4.72 \pm 0.06)e-13	(1.63 \pm 0.15)e-14	29.0 \pm 2.7	(3.19 \pm 0.33)e-14	14.8 \pm 1.5	(1.77 \pm 0.02)e-12	0.267 \pm 0.004
2004 May 24	(5.21 \pm 0.05)e-13	(1.49 \pm 0.15)e-14	35.0 \pm 3.5	(2.00 \pm 0.13)e-14	26.1 \pm 1.8	(2.00 \pm 0.04)e-12	0.261 \pm 0.006
2006 Jan 9	(5.89 \pm 0.02)e-13	(1.02 \pm 0.06)e-14	57.8 \pm 3.6	(1.70 \pm 0.07)e-14	34.7 \pm 1.4	(1.57 \pm 0.02)e-12	0.375 \pm 0.005
2006 Jun 20	(4.19 \pm 0.04)e-13	(7.30 \pm 0.59)e-15	57.4 \pm 4.7	(1.65 \pm 0.10)e-14	25.4 \pm 1.5	(1.30 \pm 0.02)e-12	0.322 \pm 0.005
2007 Feb 17	(2.97 \pm 0.03)e-13	(4.29 \pm 0.43)e-15	69.2 \pm 7.0	(8.04 \pm 0.90)e-15	36.9 \pm 4.1	(1.04 \pm 0.01)e-12	0.286 \pm 0.005

cance of the coronal line variability. Then, we have measured the fluxes of the two prominent broad emission lines Pa β (in the near-IR) and H α (in the optical). Since the BELR is expected to be the most variable of any AGN emission line region, the observed flux *increase* of these broad lines gives an estimate of the maximum value that can be reached within the current data set. These results are also listed in Tables 1 and 2.

In addition to the emission lines, we have measured in the near-IR spectra the continuum fluxes at the rest-frame wavelengths of $\sim 1\mu\text{m}$ and $\sim 2.1\mu\text{m}$ (see Table 3). As we have shown in Landt et al. (2011), the former is dominated by the accretion disc flux, which is believed to be the main source of ionising radiation in AGN and so the driver of the observed variability, whereas the latter is emitted from the hot dust component of the obscuring torus. Furthermore, we have derived the hot dust temperature from black-body fits to the near-IR spectral continuum as described in Landt et al. (2011) and list it also in Table 3. In Section 4, we will compare these values to the optical coronal line ratios [Fe VII] $\lambda 6087/\lambda 3759$ and [Fe VII] $\lambda 5159/\lambda 6087$, which are suitable indicators of the gas temperature and density (Nussbaumer et al. 1982; Keenan & Norrington 1987), respectively (listed in Table 3).

2.2 X-ray spectroscopy

As one of the brightest Seyfert 1 galaxies at X-ray frequencies, NGC 5548 was intensively studied in the years 1999-2002, after which period the source became unobservable by *XMM-Newton* and had only limited observability with *Chandra*. Due to the limited observability, there are two shorter *Chandra* observations in 2005 and 2007, until a long observational campaign took place in the summer of 2013 and winter of 2013/14. Between 2002 and 2007, the time period overlapping with our near-IR and optical spectroscopy, there are a total of three *Chandra* observations of NGC 5548 with the low-energy transmission grating in combination with the high-resolution camera spectrograph (LETGS). The 2002 observations showed the source in an average flux state, while the 2005 and especially the 2007 spectra were obtained in low-flux states. The exposure times were 340 ks, 141 ks and 162 ks in 2002, 2005, and 2007, respectively. All three X-ray observations were taken over a period of three days during two consecutive orbits. The low flux state helps in the detection of emission lines but the shorter exposure times lead to low S/N spectra.

The X-ray spectra obtained between 2002 and 2007 were analysed by Steenbrugge et al. (2005), Detmers et al. (2008, 2009) and, most recently, Ebrero et al. (2015, in

Table 3. Near-IR continuum fluxes and optical coronal line ratios

Observation Date	$\lambda f_{1\mu\text{m}}$ (erg/s/cm ²)	$\lambda f_{1\mu\text{m}}/$ [S III]	$\lambda f_{2.1\mu\text{m}}$ (erg/s/cm ²)	$\lambda f_{2.1\mu\text{m}}/$ [S III]	T_{dust} (K)	[Fe VII] $\lambda 6087/$ [Fe VII] $\lambda 3759$	[Fe VII] $\lambda 5159/$ [Fe VII] $\lambda 6087$
2002 Apr 23	(7.74 \pm 0.08)e-12	277.4 \pm 6.7	(1.38 \pm 0.01)e-11	494.6 \pm 10.9	1371	1.644 \pm 0.268	0.348 \pm 0.071
2004 May 23	(1.48 \pm 0.07)e-11	328.9 \pm 17.1	(1.85 \pm 0.02)e-11	411.1 \pm 11.5	1572	1.031 \pm 0.129	0.645 \pm 0.082
2006 Jan 9	(2.38 \pm 0.09)e-11	616.6 \pm 43.2	(2.68 \pm 0.04)e-11	694.3 \pm 41.7	1730	1.241 \pm 0.128	0.489 \pm 0.062
2006 Jun 12	(2.32 \pm 0.06)e-11	357.5 \pm 11.8	(3.56 \pm 0.02)e-11	548.5 \pm 13.2	1547	0.892 \pm 0.105	0.547 \pm 0.069
2007 Jan 24	(2.10 \pm 0.04)e-11	391.8 \pm 11.0	(2.19 \pm 0.02)e-11	408.6 \pm 8.2	1291	0.918 \pm 0.166	0.627 \pm 0.112

Table 4. X-ray emission line and continuum fluxes

Observation Date	O VII f 0.561 keV*		$f_{0.2-10\text{keV}}$
	Ebrero et al. (ph/s/cm ²)	Detmers et al. (ph/s/cm ²)	Ebrero et al. (erg/s/cm ²)
2002 Jan 18	(0.83 \pm 0.07)e-04	(0.75 \pm 0.07)e-04	(1.51 \pm 0.02)e-10
2005 Apr 15	(0.42 \pm 0.07)e-04	(0.35 \pm 0.06)e-04	(1.90 \pm 0.06)e-11
2007 Aug 14	(0.34 \pm 0.07)e-04	(0.27 \pm 0.06)e-04	(1.05 \pm 0.06)e-11

* Ebrero et al. contrary to Detmers et al. assume that the narrow emission lines are absorbed by the warm absorber.

prep.). Both Detmers et al. (2009) and Ebrero et al. analyse all previously observed X-ray spectra using the latest atomic data. The difference between the two is that Ebrero et al. focus on detecting changes in the warm absorber with continuum flux level and so, contrary to Detmers et al. (2009), assume that the narrow emission lines are absorbed by the warm absorber. Generally, it has been assumed that the warm absorber does not affect the flux of the narrow emission lines, however, Whewell et al. (2015, submitted) have recently presented evidence that at least one and potentially up to three warm absorber components do indeed absorb at least the O VII triplet and most likely all narrow X-ray emission lines. In Table 4, we list the measurements and their 1σ errors from both studies, Ebrero et al. and Detmers et al., which yield similar results. Due to the still rather high continuum level in 2005 and 2007 and lower S/N in 2005, only the O VII f narrow emission line was detected in all three spectra.

3 THE VARIABILITY BEHAVIOUR

3.1 The near-IR and optical coronal lines

Over the ~ 5 year period sampled by the near-IR and optical spectroscopy the ionising flux of the accretion disc, which is assumed to be the main driver for the variability of the broad line, coronal line and hot dust emission regions, stayed constant in the first two years, increased by a factor of ~ 2 in the following two years and decreased again to its original flux state during the last year (see Fig. 1). We note that the flux increase of $\sim 19\%$ observed between the April 2002 and May 2004 epochs is consistent with zero, once the deviations from the theoretical value of the [S III] $\lambda 9531$ /[S III] $\lambda 9069$ ratios measured in these spectra are taken into account ($\sim 14.8\%$ and $\sim 1.1\%$, respectively). The variability of the ionising continuum is mirrored in that of the hot dust emission and Pa β broad line region (see Figs. 1 and 2, respectively); also their flux stayed constant in the first two years, increased

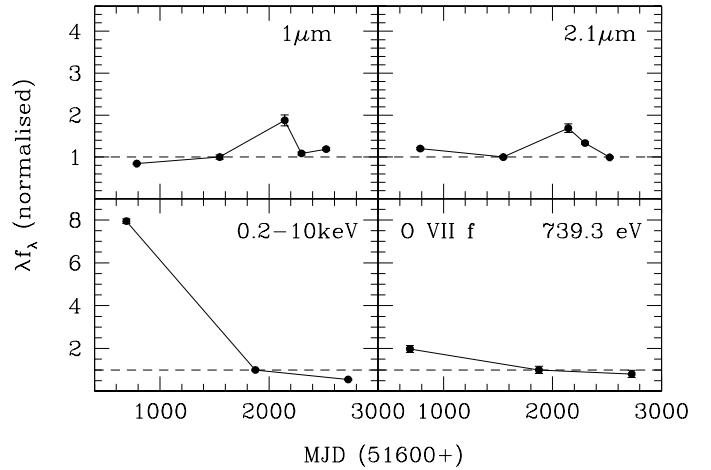


Figure 1. The variability of the continuum fluxes at rest-frame wavelengths of $\sim 1 \mu\text{m}$ (sampling the accretion disc), $\sim 2.1 \mu\text{m}$ (sampling the hot dust emission) and in the energy range $0.2 - 10 \text{ keV}$ (related to the accretion disc) and that of the O VII f X-ray coronal line. The near-IR continuum fluxes were divided by the [S III] $\lambda 9531$ line flux and normalised to the value of the May 2004 epoch. The X-ray measurements were normalised to the value of the April 2005 epoch. Note the different y-axis scale in the bottom two panels. We plot 1σ error bars.

in the following two years (by $\sim 70\%$ and $\sim 30\%$, respectively), and then continuously decreased to its original level for the next year. The flux of the H α broad line region also stayed constant in the first two years, but then decreased in the next two years (by $\sim 40\%$), followed by an increase to its original level during the last year.

The variability response of the near-IR coronal lines was stronger than that of the hot dust emission and broad emission line region and in general very different from it. Whereas the flux of the [S IX] and [Si X] lines, the lines with the highest ionisation potentials, stayed constant in the first

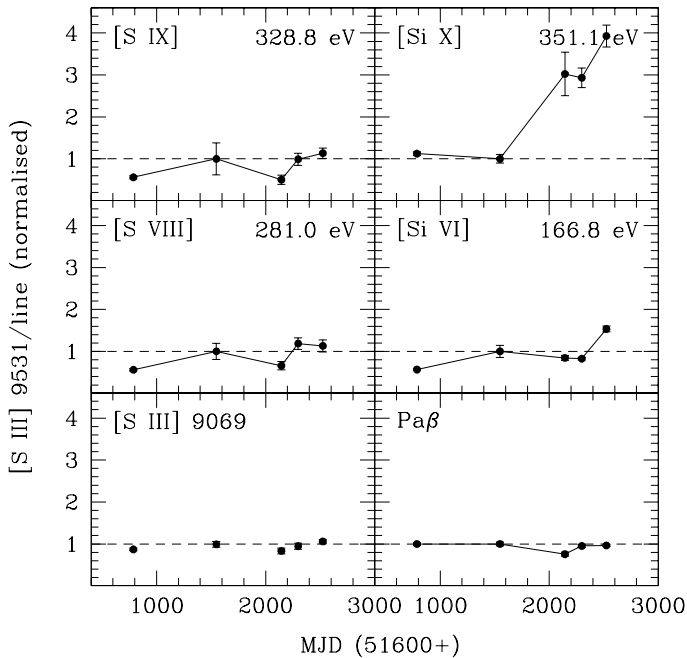


Figure 2. The variability of the near-IR coronal lines in the period April 2002 - January 2007. For comparison, we show also the [S III] $\lambda 9069$ narrow line and Pa β broad line, which are expected not to vary and to vary maximally, respectively. The [S III] $\lambda 9531$ /[S III] $\lambda 9069$ flux ratios were normalised to the theoretical value, whereas those between [S III] $\lambda 9531$ and the other lines were normalised to the value of the May 2004 epoch. We plot 1σ error bars. The ionisation potentials of the coronal lines are given at the top right.

two years, the flux of the other two near-IR coronal lines decreased by a factor of ~ 2 . After this initial decrease, the flux of the [S VIII] line stayed constant, whereas the flux of the [Si VI] line stayed constant in the following two years, but decreased further in the last year, resulting in a total decrease during the observing period of a factor of ~ 3 . The flux of the [S IX] line decreased significantly (by a factor of ~ 2) only during the last year of the observing period, whereas the [Si X] line started to diminish already in May 2004 and by the end of the observing period reached a flux decrease of a factor of ~ 4 .

Similarly to the [S VIII] and [Si VI] near-IR coronal lines, the flux of the optical coronal line [Fe VII] $\lambda 6087$ decreased by $\sim 80\%$ in the first two years, whereas the flux of the other three [Fe VII] lines stayed constant. The flux of the [Fe VII] $\lambda 6087$ line further decreased in the following two years (by $\sim 30\%$), then increased and decreased again, thus reaching a flux decrease of a factor of ~ 2 by the end of the observing period. Similarly to the H α broad line, the flux of the [Fe VII] $\lambda 5159$ line, after staying constant for the first two years, decreased in the following two years (by $\sim 80\%$), followed by an increase to its original level during the last year. Similarly to the [Si X] near-IR coronal line, the flux of the [Fe VII] $\lambda 5721$ line started to diminish in May 2004 and by the end of the observing period reached a flux decrease of a factor of ~ 2 . Finally, after May 2004, the [Fe VII] $\lambda 3759$ line varied similarly to the [Fe VII] $\lambda 6087$ line;

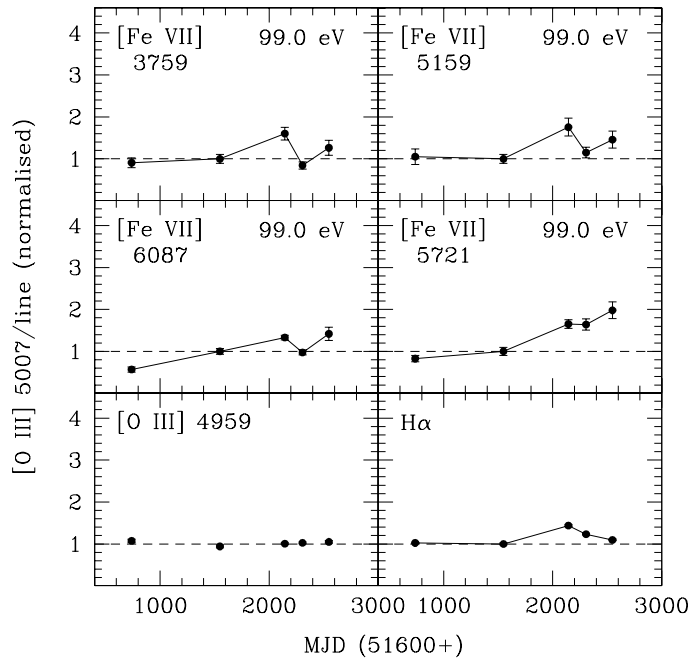


Figure 3. Same as Fig. 2 for the optical coronal lines. For comparison, we show also the [O III] $\lambda 4959$ narrow line and H α broad line, which are expected not to vary and to vary maximally, respectively.

a flux decrease by $\sim 60\%$ followed by a flux increase (by $\sim 90\%$) and then flux decrease (by $\sim 50\%$).

3.2 The X-ray coronal lines

In the ~ 5 year period sampled by the X-ray spectroscopy the unabsorbed 0.2 – 10 keV continuum flux, which is assumed to be produced by the central ionising source and so to be linked to the accretion disc flux, decreased by a factor of ~ 8 in the first three years, and then decreased further by a factor of ~ 2 in the next two years (see Fig. 1).

The variability response of the forbidden X-ray coronal line O VII f was similar to that of the near-IR and optical coronal lines (see Fig. 1). Its line flux decreased in the first three years by a factor of ~ 2 and stayed constant in the next two years. We note that this result is independent of the assumption of whether the X-ray narrow lines are affected by the warm absorber, since the ratio between the absorbed and unabsorbed line flux is similar for all three observing epochs. Detmers et al. (2008) list also the flux or non-detection limit for the Ne IX f line, which is detected only in the 2002 spectrum. The trend for this much weaker X-ray emission line is similar to that observed for the O VII f line; a decrease in flux during the observing period by a factor of $\gtrsim 3$. Finally, it is worth noting that the flux of both the O VII f line and the unabsorbed X-ray continuum recovered by the summer of 2013 to a level only slightly below that observed in 2002 (Kaastra et al. 2014).

4 THE ORIGIN OF THE CORONAL LINE EMISSION REGION

The current understanding is that the coronal line region in AGN is dust-free, photoionised and located beyond the BELR at distances from the central ionising source similar to those of the hot inner face of the obscuring dusty torus. In Landt et al. (2015) we confirmed for the source NGC 4151 that the coronal line region is photoionised but showed that it is located well beyond the hot dusty torus, at a distance from the central ionising source of a few light-years. This explained the low variability amplitude observed for the coronal lines in this source.

The situation in the source NGC 5548 seems at first glance to be very different. Whereas the broad emission lines changed only little (by $\sim 30 - 40\%$) in the period covered by our data and the hot dust emission changed moderately (by $\sim 70\%$), the coronal lines varied strongly (by factors of $\sim 2 - 4$). However, the observed high variability amplitude of the coronal lines is mainly due to a flux decrease. In fact, none of the coronal lines reacted with a flux increase to the increase in ionising flux observed between the May 2004 and January 2006 epochs as the $\text{Pa}\beta$ broad line and hot dust emission did.

In the following, we show that the coronal line region in NGC 5548 is similar to that in NGC 4151, i.e. it is a separate entity, most likely an X-ray heated wind, that has a low density and a high ionisation parameter and that is located far away from the dusty torus (Section 4.1). However, this wind appears to be stronger in NGC 5548 than in NGC 4151 and so, most likely, it undergoes a more severe adiabatic expansion and cooling after being launched (Section 4.2). Finally, in Section 4.3, we discuss the source NGC 5548 in the context of stellar tidal disruption events, which have been proposed as an alternative explanation for the fact that strong coronal line emitters often show a strong fading of their coronal lines over a period of several years.

4.1 Plasma diagnostics and the similarity between NGC 5548 and NGC 4151

As in Landt et al. (2015), we estimate the density of the coronal line gas using the three optical iron lines $[\text{Fe VII}] \lambda 3759$, $[\text{Fe VII}] \lambda 5159$ and $[\text{Fe VII}] \lambda 6087$, since, as discussed by previous studies, the line ratios $[\text{Fe VII}] \lambda 6087/\lambda 3759$ and $[\text{Fe VII}] \lambda 5159/\lambda 6087$ are suitable indicators of temperature and density, respectively (Nussbaumer et al. 1982; Keenan & Norrington 1987). For these emission lines, we have generated a temperature versus density grid using version 13.03 of the plasma simulation code CLOUDY (last described by Ferland et al. 2013) (see Fig. 4). For the photoionisation simulations we have assumed solar abundances as given by Grevesse et al. (2010) and approximated the incident radiation field with the mean AGN spectral energy distribution (SED) derived by Mathews & Ferland (1987). Recently, Mehdipour et al. (2015) observed the hard X-ray portion of the SED and found that it continues to rise, in νf_ν , until at least ~ 80 keV. So NGC 5548 was in a very hard state when their observations were done. Very hard X-rays actually have only modest effects on the physical conditions within a photoionised cloud due to their small photoelectric cross sec-

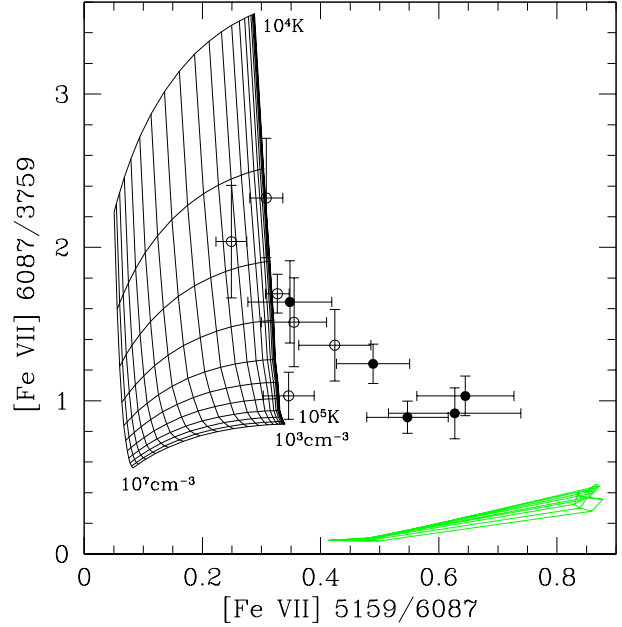


Figure 4. The observed optical coronal line ratios $[\text{Fe VII}] \lambda 6087/\lambda 3759$ versus $[\text{Fe VII}] \lambda 5159/\lambda 6087$ for NGC 5548 (filled circles) and NGC 4151 (open circles), overlaid with curves of constant temperature ($\log T = 4, 4.1, 4.2, \dots$ K) and constant number density ($\log n_e = 3, 3.2, 3.4, \dots$ cm^{-3}) for the case of photoionisation equilibrium. The case of collisional ionisation equilibrium is shown in green. We plot 1σ error bars.

tion. The emission line spectrum is mainly affected by the FUV/XUV part of the SED, which is not directly observable except in the very highest redshift objects (Collinson et al. 2015). The FUV/XUV part of the older SED was derived from line observations which were sensitive to that portion of the spectrum. The two SEDs are in qualitative agreement in this part of the spectrum, so our results would not have changed had we used the newest observations. We have assumed the cases of either photoionisation or collisional ionisation equilibrium.

The measurements for NGC 5548 (filled circles) give a similar answer to those for NGC 4151 (open circles); the coronal line gas is photoionised rather than collisionally ionised and its density appears to be relatively low. All but one observing epochs for NGC 5548 constrain it to $n_e \sim 10^3 \text{ cm}^{-3}$ within $\sim 3\sigma$, whereas the May 2004 epoch reaches this value within $\sim 4\sigma$. We note that the estimated density is several orders of magnitude below the critical density of $[\text{Fe VII}]$ of $n_{\text{crit}} \sim 3 \times 10^7 \text{ cm}^{-3}$. We find again for NGC 5548, as we did previously for NGC 4151, that all measured $[\text{Fe VII}]$ ratios lie to the right of the theoretical grids. This indicates most likely a large ionisation parameter, since in such a case the contribution from fluorescence increases significantly the $[\text{Fe VII}] \lambda 5159/\lambda 6087$ ratio (see Fig. 7 in Landt et al. 2015).

As in Landt et al. (2015), we estimate the ionisation parameter of the coronal line gas using the three X-ray lines from the helium-like ion of oxygen O VII f , O VII i and O VII r . Using the plasma simulation code CLOUDY, we have generated a ionisation parameter versus density grid for the

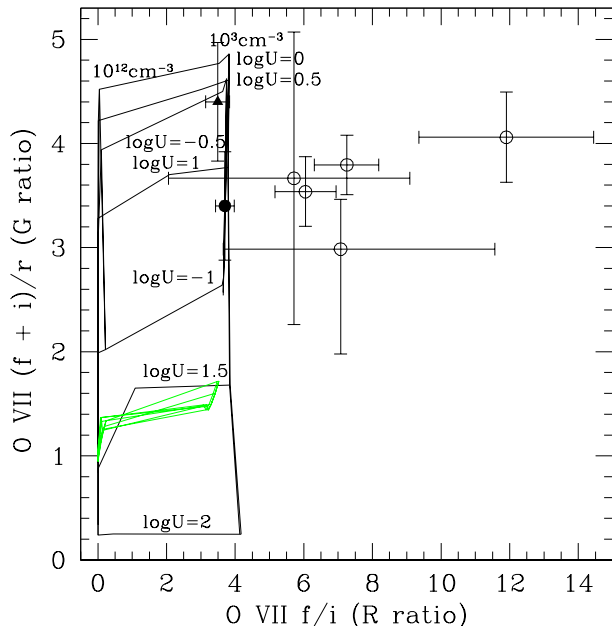


Figure 5. The observed X-ray coronal line ratios O VII (f+i)/r (G ratio) versus O VII f/i (R ratio) for NGC 5548 (filled symbols) and NGC 4151 (open circles), overlaid with curves of constant ionisation parameter ($\log U = -1, -0.5, 0, \dots, 2$) for two constant number densities ($n_e = 10^3 \text{ cm}^{-3}$ and $n_e = 10^{12} \text{ cm}^{-3}$) and a fixed column density of $N_H = 10^{21} \text{ cm}^{-2}$, assuming photoionisation equilibrium. For NGC 5548 we plot both the absorbed (filled circle) and unabsorbed case (filled triangle). The case of collisional ionisation equilibrium is shown in green. We plot 1σ error bars.

O VII lines (see Fig. 5). As discussed by previous studies, the X-ray line ratios O VII (f+i)/r (the so-called G ratio) and O VII f/i (the so-called R ratio) trace the ionisation parameter, which is directly related to the kinetic gas temperature, and density, respectively, for a given column density (Porquet & Dubau 2000; Porter & Ferland 2007). We assumed again the cases of either photoionisation or collisional ionisation equilibrium. Neither of the studies mentioned in Section 2.2 detects all three O VII lines and, therefore, no density and/or ionisation parameter can be determined from this triplet for the period 2002–2007. However, the entire O VII triplet is detected by Kaastra et al. (2014) when the source was in an obscured state similar to what is generally observed for NGC 4151. Kaastra et al. (2014) assumed that the narrow emission lines are not absorbed by the warm absorber (similar to the study of Detmers et al. 2009) and from their data we determine a G ratio of 4.40 ± 0.57 and an R ratio of 3.49 ± 0.35 (filled triangle in Fig. 5). Andrade-Velázquez et al. (2010) combined all *Chandra* spectra taken before 2007 and measure the O VII triplet in the stacked HETG and LETG spectra, also assuming that the lines are not absorbed by the warm absorber. From their data we calculate a G ratio of $8.8^{+6.2}_{-6.1}$ and $4.6^{+2.8}_{-1.4}$ and an R ratio of $3.3^{+1.5}_{-1.4}$ and $2.8^{+1.5}_{-0.6}$ for the HETG and LETG data, respectively. Given the large errors, these results are consistent with the *XMM-Newton* results of Kaastra et al. (2014). Therefore, we will use here the latter data given the higher quality, although the observations are not contemporaneous with our optical spectroscopy.

If we assume that the O VII triplet is affected by the warm absorber, both the G and R ratios decrease, because the resonance and intercombination lines are absorbed whereas the forbidden line is not. Mehdipour et al. (2015) have recently pointed out that inner shell lines of O VI can absorb components of the O VII lines used as a diagnostic here and in observations of NGC 4151 presented in Landt et al. (2015). This hypothesis is attractive because it is hard to think of any other way to account for the unusual ratios found in our previous paper. But the problem with their explanation in the case of NGC 5548 is that the measured O VI column density ($N_{\text{OVI}} = 10^{16} \text{ cm}^{-2}$; Steenbrugge et al. 2005) of the warm absorber, which potentially can be cospatial with the O VII line emitting region, is ~ 1.5 dex smaller than that needed to produce the absorption assuming their atomic data. Then, using the line strengths from Whewell et al. (2015, submitted), the G and R ratios become 3.40 ± 0.52 and 3.70 ± 0.27 , respectively (filled circle in Fig. 5). The absorbed values constrain the ionisation parameter of the coronal line gas in NGC 5548 to $\log U \sim 1$, as found previously for NGC 4151.

Then, using the unabsorbed X-ray luminosity of $L_{2-10\text{keV}} \sim 4 \times 10^{43} \text{ erg s}^{-1}$ of the highest-flux epoch as a proxy for the ionising luminosity producing O VII and the best-fit X-ray spectral slope of this epoch of $\Gamma \sim 1.88$ (Steenbrugge et al. 2005) to estimate the mean ionising photon energy, the calculated distance of the coronal line region in NGC 5548 from the central ionising source for the above gas density is $\tau_t \sim 2850$ light days ~ 7.8 light years. As found previously for NGC 4151, this value places this region well beyond the hot inner face of the obscuring dusty torus, which in NGC 5548 is measured by dust reverberation campaigns to be $\sim 40 - 60$ days (Koshida et al. 2014). Furthermore, it is consistent with the fact that a recovery of the flux of the coronal lines to the high level seen in the 2002 epoch is occurring only in 2013 (see Section 3.2) and that only a flux decrease is observed in the 5-yr time period spanned by our own data set.

4.2 The X-ray heated wind scenario and the difference between NGC 5548 and NGC 4151

Pier & Voit (1995) proposed that the coronal line region is a layer on the inner part of the dusty torus that becomes an efficient coronal line emitter only when evaporated in an X-ray heated wind. In this scenario, the wind will have undergone adiabatic expansion from its launch location at the inner face of the torus until the gas density and distance from the ionising source are optimal to give the required high ionisation parameter. In the process, the coronal line gas will have cooled. In Fig. 6 we present tentative evidence that this scenario applies to NGC 5548, similar to what we found previously for NGC 4151. In the bottom panel, we compare the temperature of the coronal line gas as measured by the line ratio $[\text{Fe VII}] \lambda 6087 / [\text{Fe VII}] \lambda 3759$ (the higher its value, the lower the gas temperature; see Fig. 4) with that of the hot dust. We find that the two temperatures behave in opposite ways; the temperature of the coronal line gas is high when the hot dust temperature is low and vice versa. Only the data from April 2002 is an exception to this trend and might indicate a reddening event. In the top panel of Fig. 6, we show the continuum flux at rest-frame wavelength of

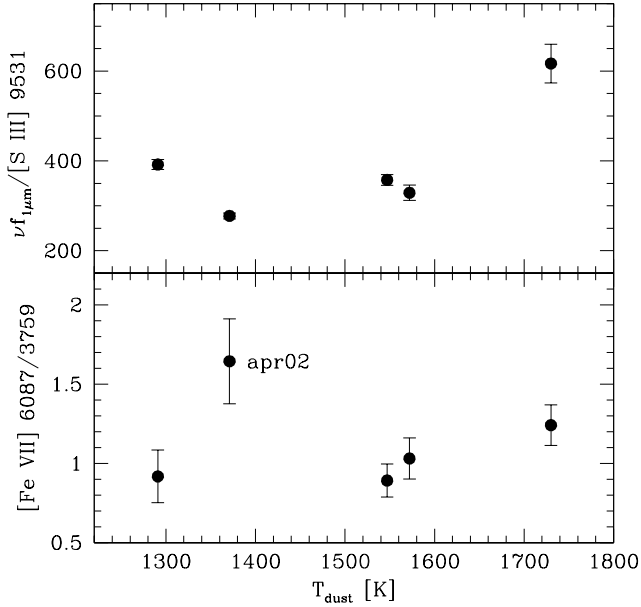


Figure 6. The top and bottom panels show the continuum flux at rest-frame wavelength of $\sim 1 \mu\text{m}$ (sampling the accretion disc) scaled to the $[\text{S III}] \lambda 9531$ line flux and the optical coronal line ratio $[\text{Fe VII}] \lambda 6087/\lambda 3759$, which is a suitable indicator of the gas temperature (the higher its value, the lower the temperature; see Fig. 4), respectively, versus the hot dust blackbody temperature.

$\sim 1 \mu\text{m}$, which samples the accretion disc luminosity, versus the hot dust temperature. A clear correlation is apparent, which indicates that the change in temperature for the hot dust is due to direct heating by the central ionising source. Therefore, the increased AGN radiation that heats the dusty torus also increases the cooling of the coronal line gas.

In the scenario of Pier & Voit (1995), the dusty clouds will be evaporated in an X-ray heated wind more efficiently for higher AGN luminosities, which will lead to both an increase in mass outflow rate and a stronger adiabatic expansion. We observe this effect individually for NGC 5548 and NGC 4151, but it seems to also apply when comparing the two sources with each other. The coronal lines in NGC 5548 are a factor of $\sim 3 - 5$ stronger than in NGC 4151 relative to the low-ionisation narrow emission lines, and so are both the $\sim 1 \mu\text{m}$ and $\sim 2.1 \mu\text{m}$ luminosities (higher by a factor of ~ 3 and ~ 2 , respectively). This indicates that the X-ray heated wind producing the coronal lines in NGC 5548 is stronger than that in NGC 4151, in which case we also expect a stronger adiabatic expansion. The much stronger fading of the coronal lines with time observed for NGC 5548 relative to NGC 4151 is most likely a manifestation of it.

4.3 Strong coronal line emitters as stellar tidal disruption events

Such a strong variability of the coronal lines, i.e. fading of the flux, as we observe for NGC 5548 has been reported so far for only one AGN (IC 3599; Grupe et al. 1995; Brandt et al. 1995) and is usually associated with a new class of non-active galaxies, the so-called strong coronal line emitters. Several of these sources have recently been detected in the SDSS

(Komossa et al. 2008; Gelbord et al. 2009; Komossa et al. 2009; Wang et al. 2011, 2012; Yang et al. 2013; Rose et al. 2015). A stellar tidal disruption event seems to be the most plausible explanation for the strong fading of the coronal lines observed in these sources over a time period of several years. The tidal disruption of a star by a supermassive black hole produces an accretion event, a flare, that subsequently fades on timescales of several months to a year. The accretion flare is seen as an X-ray/UV outburst, which can produce highly ionised emission lines, including emission from He II. The X-ray luminosity outburst is expected to fade with time as $t^{-5/3}$ or slightly shallower than this depending on the type of the star (Rees 1988; Phinney 1989; Lodato et al. 2009) and subsequently a strong fading of the high-ionisation lines is expected.

Could the strong coronal line variability that we observe for NGC 5548 have been caused by a stellar tidal disruption event? Such an event was raised as a possibility for the strong increase (by a factor of $\gtrsim 10$) of the He II $\lambda 4686$ emission line flux observed for this source between January and May 1984 by Peterson & Ferland (1986) and interpreted as the addition of a new gas component unrelated to the BELR. The recently discovered strong coronal line emitters have line ratios $[\text{Fe VII}] \lambda 6087/[\text{O III}] \lambda 5007 \sim 0.1 - 1$ and have $[\text{Fe X}]$ emission comparable to or stronger than $[\text{Fe VII}]$ before the fading of the lines. In NGC 5548, we measure line ratios $[\text{Fe VII}] \lambda 6087/[\text{O III}] \lambda 5007 \sim 0.03 - 0.07$, which puts this source in the vicinity of the strong coronal line emitters. However, the $[\text{Fe X}] \lambda 6375$ emission line is a factor of ~ 5 weaker than the $[\text{Fe VII}] \lambda 6087$ emission line. As expected for stellar tidal disruption events, the high-state of the coronal lines in 2002 is accompanied by a high state of the X-ray flux, which subsequently fades strongly. The observed X-ray flux decrease of a factor of ~ 8 in 3 years roughly obeys the expected $t^{-5/3}$ decay law for these events (albeit based on only two points). However, the flux of both the X-ray continuum and O VII f X-ray coronal line are observed to have recovered by 2013 to their original high state (see Section 3.2). Finally, the He II emission line did not show the continuous flux decline observed for most of the coronal lines. Its flux varied significantly during the observing period, but fluctuated between increase and decrease from epoch to epoch. Given these considerations, it is therefore unlikely that the strong coronal line variability that we observe for NGC 5548 was caused by a stellar tidal disruption event.

5 SUMMARY AND CONCLUSIONS

We have presented the second extensive study of the coronal line variability in an AGN. Our data set for the well-studied source NGC 5548 is unprecedented in that it includes five epochs of quasi-simultaneous optical and near-IR spectroscopy spanning a period of ~ 5 years and three epochs of X-ray spectroscopy overlapping in time with it. Our main results are as follows.

- (i) Whereas the broad emission lines changed only little (by $\sim 30 - 40\%$) and the hot dust emission changed moderately (by $\sim 70\%$), the coronal lines varied strongly (by factors of $\sim 2 - 4$). However, the observed high variability amplitude of the coronal lines is mainly due to a flux decrease. In fact, none of the coronal lines reacted with a flux

increase to the increase in ionising flux observed between the May 2004 and January 2006 epochs as the Pa β broad line and hot dust emission did.

(ii) We have applied plasma diagnostics to the optical [Fe VII] and X-ray O VII emission lines in order to constrain the gas number density, temperature and ionisation parameter of the coronal line region. We find that this gas has a relatively low density of $n_e \sim 10^3 \text{ cm}^{-3}$ and requires a relatively high ionisation parameter of $\log U \sim 1$, similar to our previous results for the source NGC 4151. We estimate the distance of the coronal line region in NGC 5548 from the central ionising source for the above gas density to be $\tau_t \sim 7.8$ light years. This value puts this region well beyond the hot inner face of the obscuring dusty torus (of ~ 2 light months; Koshida et al. 2014).

(iii) The relatively high ionisation parameter at large distances make it likely that the coronal line region is an independent entity. One possibility is that it is an X-ray heated wind as first proposed by Pier & Voit (1995). As in the case of NGC 4151, we find support for this scenario in the form of a temperature anti-correlation between the coronal line gas and hot dust, which indicates that the increased AGN radiation that heats the dusty torus appears to increase the cooling efficiency of the coronal line gas, most likely due to a stronger adiabatic expansion. The strong coronal line variability of NGC 5548 can also be explained within this picture; relative to the low-ionisation narrow emission lines the coronal lines in NGC 5548 are a factor of $\sim 3-5$ stronger than those in NGC 4151 indicating a much stronger wind, in which case a stronger adiabatic expansion of the gas and so fading of the line emission is expected.

(iv) Since NGC 5548 can be classified as a strong coronal line emitter, we investigate if the strong coronal line variability could have been caused by a stellar tidal disruption event, as is often proposed for this kind of sources. Given that the flux of both the X-ray continuum and O VII f X-ray coronal line are observed to have recovered by 2013 to their original high state and that the He II emission line did not show the continuous flux decline observed for most of the coronal lines, we consider this scenario an unlikely explanation for the strong coronal line variability.

ACKNOWLEDGMENTS

HL is supported by a European Union COFUND/Durham Junior Research Fellowship (under EU grant agreement number 267209). KCS thanks the astronomy group at Durham University for its hospitality during a collaborative visit. GJF acknowledges support by NSF (1108928, 1109061, and 1412155), NASA (10-ATP10-0053, 10-ADAP10-0073, NNX12AH73G, and ATP13-0153), and STScI (HST-AR-13245, GO-12560, HST-GO-12309, GO-13310.002-A, and HST-AR-13914), and to the Leverhulme Trust for support via the award of a Visiting Professorship at Queen's University Belfast (VP1-2012-025).

REFERENCES

- Andrade-Velázquez, M., Krongold, Y., Elvis, M., Nicastro, F., Brickhouse, N., Binette, L., Mathur, S., & Jiménez-Bailón, E. 2010, *ApJ*, 711, 888
- Appenzeller, I., & Oestreicher, R. 1988, *AJ*, 95, 45
- Brandt, W. N., Pounds, K. A., & Fink, H. 1995, *MNRAS*, 273, L47
- Collinson, J. S., Ward, M. J., Done, C., Landt, H., Elvis, M., & McDowell, J. C. 2015, *MNRAS*, 449, 2174
- Detmers, R. G., Kaastra, J. S., Costantini, E., McHardy, I. M., & Verbunt, F. 2008, *A&A*, 488, 67
- Detmers, R. G., Kaastra, J. S., & McHardy, I. M. 2009, *A&A*, 504, 409
- Erkens, U., Appenzeller, I., & Wagner, S. 1997, *A&A*, 323, 707
- Fabricant, D., Cheimets, P., Caldwell, N., & Geary, J. 1998, *PASP*, 110, 79
- Ferland, G. J., et al. 2013, *RMxAA*, 49, 137
- Gelbord, J. M., Mullaney, J. R., & Ward, M. J. 2009, *MNRAS*, 397, 172
- Grevesse, N., Asplund, M., Sauval, A. J., & Scott, P. 2010, *Ap&SS*, 328, 179
- Grupe, D., Beuermann, K., Mannheim, K., Bade, N., Thomas, H.-C., de Martino, D., & Schwope, A. 1995, *A&A*, 299, L5
- Kaastra, J. S., et al. 2014, *Science*, 345, 64
- Keenan, F. P., & Norrington, P. H. 1987, *A&A*, 181, 370
- Kollatschny, W., Bischoff, K., Robinson, E. L., Welsh, W. F., & Hill, G. J. 2001, *A&A*, 379, 125
- Komossa, S., et al. 2009, *ApJ*, 701, 105
- Komossa, S., et al. 2008, *ApJ*, 678, L13
- Koshida, S., et al. 2014, *ApJ*, 788, 159
- Kramida, A., Yu. Ralchenko, Reader, J., & and NIST ASD Team. 2013, NIST Atomic Spectra Database (ver. 5.1), [Online]. Available: <http://physics.nist.gov/asd>. National Institute of Standards and Technology, Gaithersburg, MD.
- Landt, H., Bentz, M. C., Ward, M. J., Elvis, M., Peterson, B. M., Korista, K. T., & Karovska, M. 2008, *ApJS*, 174, 282
- Landt, H., Elvis, M., Ward, M. J., Bentz, M. C., Korista, K. T., & Karovska, M. 2011, *MNRAS*, 414, 218
- Landt, H., Ward, M. J., Steenbrugge, K. C., & Ferland, G. J. 2015, *MNRAS*, 449, 3795
- Lodato, G., King, A. R., & Pringle, J. E. 2009, *MNRAS*, 392, 332
- Mathews, W. G., & Ferland, G. J. 1987, *ApJ*, 323, 456
- Mazzalay, X., Rodríguez-Ardila, A., Komossa, S., & McGregor, P. J. 2013, *MNRAS*, 430, 2411
- Mehdipour, M., et al. 2015, *A&A*, 575, A22
- Mehdipour, M., Kaastra, J. S., & Raassen, A. J. J. 2015, *A&A*, 579, 87
- Müller Sánchez, F., Davies, R. I., Eisenhauer, F., Tacconi, L. J., Genzel, R., & Sternberg, A. 2006, *A&A*, 454, 481
- Müller-Sánchez, F., Prieto, M. A., Hicks, E. K. S., Vives-Arias, H., Davies, R. I., Malkan, M., Tacconi, L. J., & Genzel, R. 2011, *ApJ*, 739, 69
- Nussbaumer, H., Storey, P. J., & Storey, P. J. 1982, *A&A*, 113, 21
- Penston, M. V., Fosbury, R. A. E., Boksenberg, A., Ward, M. J., & Wilson, A. S. 1984, *MNRAS*, 208, 347
- Peterson, B. M., & Ferland, G. J. 1986, *Nature*, 324, 345
- Phinney, E. S. 1989, in *IAU Symposium*, Vol. 136, The Center of the Galaxy, ed. M. Morris, 543

- Pier, E. A., & Voit, G. M. 1995, *ApJ*, 450, 628
- Pogge, R. W. 1988, *ApJ*, 328, 519
- Porquet, D., & Dubau, J. 2000, *A&AS*, 143, 495
- Porter, R. L., & Ferland, G. J. 2007, *ApJ*, 664, 586
- Prieto, M. A., Marco, O., & Gallimore, J. 2005, *MNRAS*, 364, L28
- Rayner, J. T., Toomey, D. W., Onaka, P. M., Denault, A. J., Stahlberger, W. E., Vacca, W. D., Cushing, M. C., & Wang, S. 2003, *PASP*, 115, 362
- Rees, M. J. 1988, *Nature*, 333, 523
- Riffel, R., Rodríguez-Ardila, A., & Pastoriza, M. G. 2006, *A&A*, 457, 61
- Rodríguez-Ardila, A., Prieto, M. A., Portilla, J. G., & Tejeiro, J. M. 2011, *ApJ*, 743, 100
- Rodríguez-Ardila, A., Viegas, S. M., Pastoriza, M. G., & Prato, L. 2002, *ApJ*, 579, 214
- Rose, M., Elvis, M., & Tadhunter, C. N. 2015, *MNRAS*, 448, 2900
- Steenbrugge, K. C., et al. 2005, *A&A*, 434, 569
- Tadhunter, C., & Tsvetanov, Z. 1989, *Nature*, 341, 422
- Veilleux, S. 1988, *AJ*, 95, 1695
- Wang, T.-G., Zhou, H.-Y., Komossa, S., Wang, H.-Y., Yuan, W., & Yang, C. 2012, *ApJ*, 749, 115
- Wang, T.-G., Zhou, H.-Y., Wang, L.-F., Lu, H.-L., & Xu, D. 2011, *ApJ*, 740, 85
- Yang, C.-W., Wang, T.-G., Ferland, G., Yuan, W., Zhou, H.-Y., & Jiang, P. 2013, *ApJ*, 774, 46

This paper has been typeset from a $\mathrm{T}_{\mathrm{E}}\mathrm{X}$ / $\mathrm{L}^{\mathrm{A}}\mathrm{T}_{\mathrm{E}}\mathrm{X}$ file prepared by the author.